THESIS FOR THE DEGREE OF LICENTIATE OF ENGINEERING

Upgrading Cellulose Networks: Conquering Limitations in Fiber Foams

ELIOTT ORZAN

Department of Chemistry and Chemical Engineering
CHALMERS UNIVERSITY OF TECHNOLOGY
Göteborg, Sweden 2023

Upgrading Cellulose Networks: Conquering Limitations in Fiber Foams
ELIOTT ORZAN

Licentiatuppsatser vid Institutionen för kemi och kemiteknik

Chalmers tekniska högskola
Nr 2023:10

Department of Chemistry and Chemical Engineering
Chalmers University of Technology
SE-412 96 Gothenburg
Telephone +46 31 772 1000

Cover:
AI rendered image of the prompt "wood fiber foam competing with plastic foam" using Microsoft Bing Image Creator (DALL-E).

Printed by Chalmers Reproservice
Gothenburg, Sweden 2023

Upgrading Cellulose Networks: Conquering Limitations in Fiber Foams

ELIOTT ORZAN
Department of Chemistry and Chemical Engineering
Chalmers University of Technology

ABSTRACT

The battle to create structural materials with low environmental impact demands the investiture of two champions: porous structures and cellulose substrates. The dominant solutions when constructing strong lightweight materials are plastic and metallic foams, while currently, cellulose fiber foams suffer from challenges which hamper their development. Cellulose foams are structurally promising, but are sensitive to humidity and fire, and often have an inferior mechanical performance compared to their plastic and metallic counterparts. In addition, standard foaming techniques for cellulose fiber foams use synthetic sodium dodecyl sulfate (SDS), a surfactant which weakens critical fiber-to-fiber contacts. In this work, two approaches were employed as solutions to strengthen cellulose foams: cross-linking of cellulose fibers, and controlling pore structure formation. Phytic acid (PA), a bio-based polyphosphate, was cross-linked to cellulose fibers with the goal of improving fiber-fiber bonding and generating flame-retardancy in SDS-based cellulose foams. Controlling pore structure formation was separately achieved by dispersing tert-butanol (TBA), a water miscible amphiphile, into cellulose-water suspensions. Addition of TBA induced the formation of hierarchical structures which vastly increased the surface area and mechanical performance of dried foams. The functionalities produced by the two presented solutions expand the potential applications for cellulose foams, and serve to encourage the development of these materials as lightweight competitors in the transportation, construction and packaging sectors.

Keywords: cellulose, lightweight, porous network, flame-retardancy, cellular solid, fibers, cross-linking, pore structure.

Acknowledgements

To everyone who has supported my ideas, endeavors, and idiosyncrasies, thank you. A special thanks to my supervisor Tiina Nypelö for the opportunities and the push to pursue scientific questions in a way I could not appreciate before starting this PhD. Your dedication to science and personability has been an inspiration to all of us.

To the BreadCell members, working with such a diverse cast has created a thought-provoking, supportive and fun environment and I can't thank you enough for that. On that thread, I would also like to acknowledge the funding support my PhD work has received from the European Union's Horizon 2020 - Research and Innovation Framework Programme.

To my parents Christelle and Yannick, my deepest gratitudes go to you, as my love for science and travel was inspired by you. I know the distance is difficult but thank you for supporting my wish to come to Sweden to study. I promise to try and call more often.

To my friends and coworkers who I share my life and laughs with, I look forward to our next adventures together. And to the one person who cared enough to read this far, this last acknowledgement is just for you. Thank you.

Eliott Orzan, Göteborg, May 2023

LIST OF PUBLICATIONS

I. **Tert-butanol as a structuring agent for cellulose nanocrystal water suspensions**
Saül Llàcer Navarro, Eliott Orzan, Ratchawit Janewithayapun, Paavo Penttilä, Anna Ström, Roland Kádár and Tiina Nypelö
Manuscript

II. **Catalyst-free phosphorylation of cellulose for bio-based fire-retardant materials**
Eliott Orzan, Stefan Spirk, Aitor Barrio and Tiina Nypelö
Manuscript

AUTHOR CONTRIBUTION

I. Co-author; Responsible for conceptualization and planning of experiments with co-authors; Performed scanning electron microscopy investigations and mechanical testing; Participated in writing and editing the manuscript.

II. Main author. Responsible for conceptualization and planning of experiments with co-authors; Performed the experimental work; Wrote the first draft of the manuscript.

Nomenclature

Materials

CA	Citric acid
CMC	Carboxymethyl cellulose
CNC	Cellulose nanocrystal
CNF	Cellulose nanofiber
FR	Flame-retardant
OH	Hydroxyl functional group
PA	Phytic acid
SDS	Sodium dodecyl sulfate
TBA	Tert-butanol

Methods

BET	Brunauer-Emmett-Teller
FTIR	Fourier transform infrared spectroscopy
NMR	Nuclear magnetic resonance
SEM	Scanning electron microscope
SR	Schopper-Riegler
TGA	Thermogravimetric analysis

Contents

1

Introduction

Millions of years of evolution have slowly specialized the structural composition of living beings, adapting macro- to nano-scale features to suit certain functionalities. One of the most intricate repeating themes in nature is found in the formation of hierarchical structures.[1–4] The build-up of structures within structures creates hierarchies which, almost without exception, are formed of fibrillar networks. Fibrils often consist of polysaccharides or proteins, which bundle together to form structural units such as cellulose in wood or twisted chitin fibrils in crustacean shells.[5] The structural composition of these fibrils rather than the molecular body, allows them to bear load under impact, elevating their mechanical performance.[6]

Fibrils which enclose a space and form interconnected networks of solid faces and open cells are known as cellular solids (Figure 1.1).[7] Cellular solids, also referred to as solid foams or porous networks, are known for their superior specific* properties due to their reduced densities. As materials, they are great thermal insulators, excel as energy and sound absorbers, and are valued for their high strength to weight ratios. Applying the concept of hierarchical structuring to cellular solids creates strong lightweight structures such as those found in sea sponges (Figure 1.1c). The cellular skeleton of the sea sponge is itself porous, creating hierarchies of cellular solids within cellular solids. This optimized solution found in nature can serve as inspiration for infrastructural construction and minimizes weight and material need.[3,6,8,9] Nature's methodology of lightweight construction has been studied and adapted to engineer cellular solids from plastics and metals for use in major industries such as building, transportation and packaging. Lowering the density of materials by creating porous structures significantly reduces material consumption and the energy required for

*Specific is defined as the property value divided by the material density.

their transportation.[10,11] However, the pressures placed on the environment due to the exponentially growing need for these non-renewable materials demands bio-based solutions which can compete in the market. Therefore, it is necessary to turn back to the most abundant source of low-cost renewable cellular hierarchies: wood.

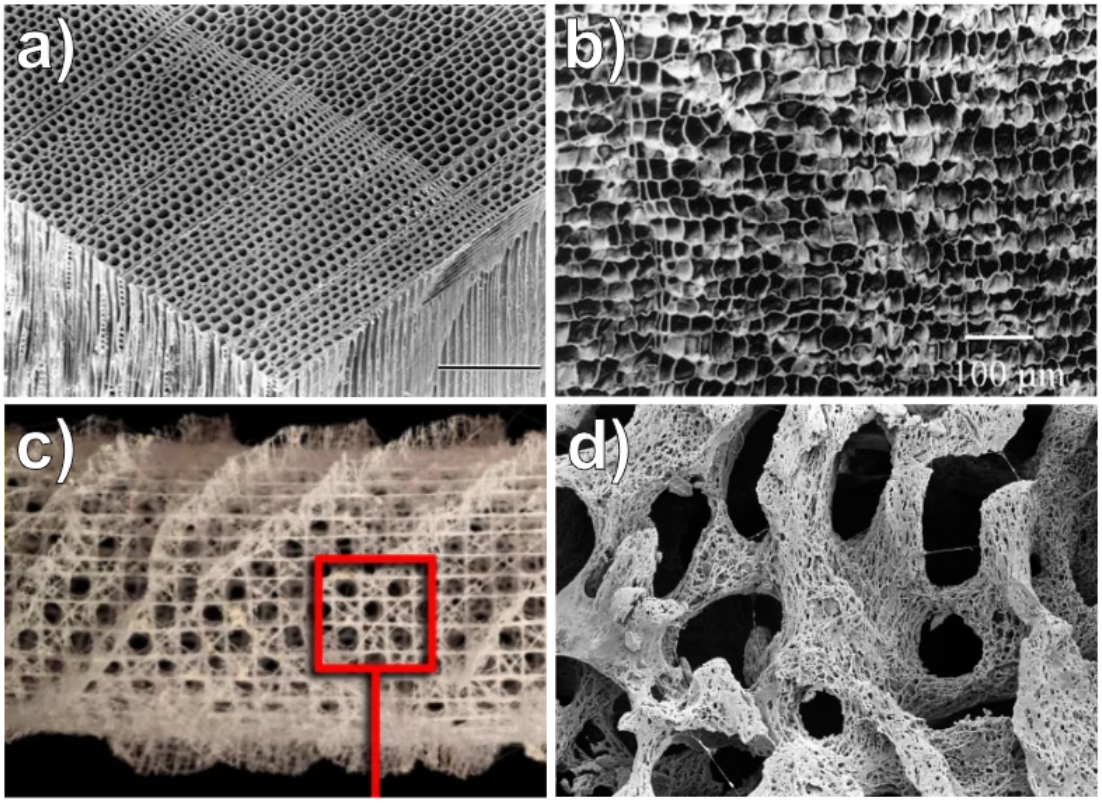

Figure 1.1: Examples of cellular solids with hierarchical structures found in nature a) wood[†], b) cork[‡], c) sea sponge[§], d) bone[¶].

The primary base structural unit of wood is cellulose, a polysaccharide chain of β-1,4-linked glucose units. Cellulose chains link together to form fibrillar hierarchies, giving wood fibers their signature strength. Each glucose unit features three hydroxyl (OH) groups, making cellulose particularly hygroscopic and thus sensitive to humidity. In addition, the poor fire resistance and poor thermal processability of cellulose fibers has created challenges which have limited their applications beyond paper and textiles. On the other hand, the presence of OH moi-

[†]Credit: C.-L. Huang et al. Springer Nature licence number: 5541851320910
[‡]Credit: Isabel Miranda et al. Springer Nature licence number: 5541861002311
[§]Credit: Matheus C. Fernandes et al. Springer Nature licence number: 5541850837784
[¶]Credit: David Gregory, Debbie Marshall. Licence: Attribution 4.0 International

eties allows cellulose surfaces to be modified via e.g. acetylation, oxidation or esterification reactions.[12] Therefore, cellulose can be easily adapted to suit certain requirements such as solubility, flame-retardancy, and material compatibility in composites. Developing cellulose fibers into foam materials tuned for structural applications presents additional challenges due to the heterogeneous nature of a fiber network. Surfactants such as SDS are employed, which creates homogeneous pore size and fiber distributions yet weakens fiber-fiber contacts.[13–18] The fibrous nature of wood pulp requires physical entanglements or other cross-links between fibers to prevent them from slipping past one another in a network under load.[19,20] To strengthen fiber-fiber bonding, conventional methods involve hot-pressing or curing of citric acid (CA) or 1,2,3,4-Butanetetracarboxylic acid, which establishes covalent bonds between fabric fibers from cellulose.[21,22]

This thesis focuses on providing solutions to strengthen fiber foam networks. The proposed chemical approach uses a similar method to citric acid cross-linking, introducing phytic acid as an alternative to enhance strength and generate fire-retardancy. Studies have verified the success of phytic acid for promoting flame-retardancy in substrates[23,24] yet the underlying mechanisms and resulting structures have been poorly elucidated. The second part of the work is focused on the physical strengthening effect of structural arrangements within foams. The use of sodium dodecyl sulfate (SDS) was replaced by introducing tert-butanol (TBA) as a pore structuring agent in cellulose nanocrystal (CNC) suspensions. The ability of TBA to disrupt the hydrogen bond network between water molecules was expected to impact the hierarchical structuring of CNC suspensions and the resulting properties of freeze-dried foams.[25,26] Therefore, it was hypothesized that modulation of TBA concentration would allow control over the porous network formation and thus properties of cellulose foams.

2

Background

The key components which underline this work are cellulose fibers and the formation of a porous network. To rival the mechanical performance of plastic foams, an understanding of how each of these components influences the structural stability is necessary. Here, the fundamental concepts behind how fiber and pore morphology lend mechanical strength to a cellulose fiber foam are elucidated and solutions are presented.

2.1 Pore formation and structural stability

A foam is defined as a dispersion of gas within a liquid, gel or solid matrix. Two foaming mechanisms are principally used to describe the formation of porous systems: dispersion and condensation methods.[27] In dispersion foams, a dispersed phase (e.g. gas) is mixed into the medium via agitation such as shaking, stirring or bubbling. Condensation foams instead rely on the dispersed phase being present as a solute in the medium, where it combines to form the gas. Once a foam has been formed, gas bubbles inside suffer from thermodynamic instabilities and begin coarsening and draining over time.[28] Coarsening describes the flow of smaller isolated gas pockets into larger bubbles due to differences in capillary pressure and the drive to reduce surface energy in the system. As bubbles rearrange and grow, the morphology of the final pore network changes, subsequently determining the properties of the dried foam. In an open-cell morphology, pores are inter-connected, allowing gas to pass through the matrix, generating properties which are ideal for thermal and sound insulation (Figure 1.1a). A closed-cell morphology instead describes isolated pores encapsulated in the matrix material, ideal for foam mechanical strength (Figure 1.1b).

Maintaining smaller pore sizes is typically advantageous for improving foam compressive strength and homogeneity.[7,18] Broad pore size distributions can create heterogeneous structures and substructures which lead to varied localized deformation behaviors. As a gas bubble increases in size, it is also increasingly affected by hydrostatic pressures from gravity and viscous traction.[27] This creates anisotropy in the gas bubbles which is an important consideration for morphological control of foam mechanical properties.[7] During axial deformation, the compressive modulus, yield stress and shear strength of the pore increases in the direction parallel to the longest cell wall.[7,29] The mechanical properties on the perpendicular axis suffer as a result of this, and thus control over the orientation and size is crucial when determining which applications each foamed material can be implemented. The most common method to keep pore sizes small is the addition of surfactants or nanoparticles, which help to stabilize the liquid-air interfaces.[15,16]

Incorporating cellulose fibers as a matrix material creates complexities which are not considered in plastic and metallic foams. The fibrillar network of cellulose fiber foams diminishes the ability for closed-cell pores to form and creates a important reliance on fiber-fiber bonding for strength. The pore size influences the density of fibers aligned in lamella between pores. With larger macropores, less material is distributed around small pores and thus fibers in the cell walls are more tightly bundled, increasing inter-fiber interactions. This causes an increase in Young's modulus, as thicker cell walls resist elastic deformation, yet also causes a decrease in yield stress with higher pore interconnectivity.[29,30] It is thought that the generation of larger pores in the matrix can due to coarsening but also local opening of fiber networks during drying.[15]

2.2 Controlling pore structure

The use of surfactant-based dispersion methods to foam cellulose fibers has strong support in literature.[15–17,28,31,32] However, templating methods have gained traction due their ability to tune hierarchical porosity. One common approach is to use ice-templating, which involves the growth of ice crystals to generated macroscopic anisotropy in freeze-dried foams.[13,30,33] Other ideas have explored oil,[29,30] wax,[34] and polymeric particles[35] as removable structuring agents.

TBA, an amphiphilic solvent, has found uses in creating foams with high specific surface areas and low thermal conductivity when dried using supercritical CO_2.[36,37] TBA disrupts hydrogen bonding between water molecules and cellulose, and creates space between fibers due to the large non-polar methyl groups.[38–40] Liquid phase structuring in TBA-water systems transforms depending on TBA concentration. At low TBA content, isolated TBA-rich regions are evenly dispersed within the aqueous phase, while at concentrations above 30 wt% there was evidence of the formation of a bicontinuous microemulsion.[25,26] Therefore it was hypothesized that TBA can also act as a hierarchical templating agent to form strong porous cellulose structures.

2.3 Fiber networks

Cellulose fibers referred to in this work are wood pulp fibers of hardwood or softwood trees. The wood is typically processed via chemical pulping processes to remove bark, lignin and other impurities. Further breakdown of pulp fibers can form cellulose nanofibers (CNFs) and highly crystalline cellulose nanocrystals (CNCs).[41] The three hierarchies of cellulose fibrils presented in Figure 2.1 have all been used extensively to form cellulose foams and each provides unique characteristics to the final material.

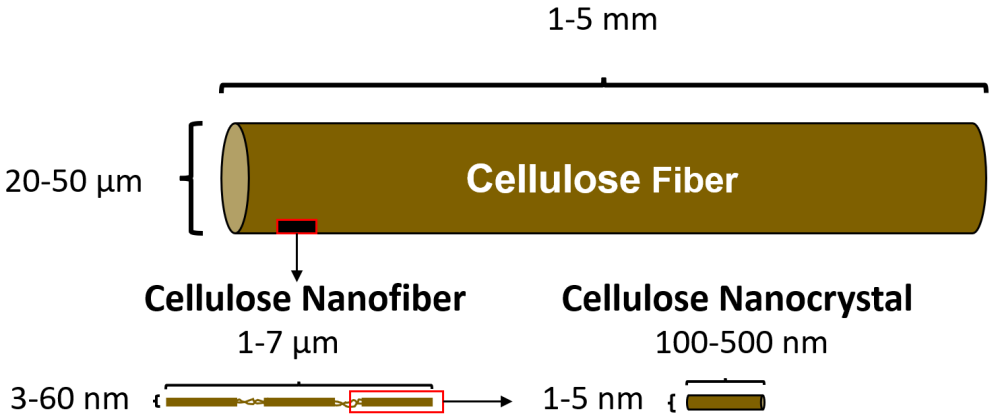

Figure 2.1: Representation of cellulose material nomenclature at different length scales. Fibrils are not drawn to scale.

The geometric structure of a foam fiber network and its properties are heavily influenced by the size, flexibility, bonding ability, and orientation of the fibers

within the network. At all fiber length scales, inter-fiber interactions such as physical entanglements and fiber-to-fiber contacts dictate the mechanical and structural strength of the foam. At lower fiber concentrations, the number of contact points between fibers lessens as as the distribution is scarcer throughout the material. Lower contact between fibers reduces the structural support a fiber can receive from neighboring fibers. In such cases, fibers may act more like individuals when load is applied as opposed to a reinforced network.[15,19] The result of this is disparate stress variations across the foam causing uneven mechanical performance. A higher fiber density in pore walls promotes fiber-fiber contacts, which increases the compressive strength of cellulose fiber foams following a power law.[7,19,20] With fiber materials of matching relative density, the pore morphology and packing density of fibers in cell walls was found to be the key criteria towards increased mechanical properties.[18,19,29]

Wood pulp fibers can help link disassociated structural areas within a foam network with their length. Yet, fibers are quite coarse and tend to exacerbate the heterogenous nature of a fiber network, creating exceedingly porous foams.[28] CNCs and CNFs by comparison are much smaller and bear higher aspect ratios. Their size creates favorable short-range fiber interactions which evenly distribute localized stresses. In addition, they can form pickering emulsions in wet foams, stabilizing gas bubbles to form homogenous pore morphologies.[18,31,42,43] However as individual units, CNCs and CNFs exhibit lower structural strength than wood pulp fibers.[19,43] Thus, fiber networks with consistently high mechanical performance and heterogeneous pore networks combined the network connectivity of CNC or CNFs with the structural reinforcement of large fibers in a foam, given that all components are well bonded in the matrix.[15,18,19,43,44] Fibrillation of wood pulp fibers and the re-introduction of fines can achieve similar effects while requiring significantly less pre-processing.[15,16]

An alternative method to physical cross-linking involves the formation of chemical cross-links between cellulose fibers. This removes the reliance on frictional forces to maintain the structural integrity of the fiber network. This method typically requires the introduction of other compounds, however provides significant strength to cellulose networks.

2.4 Chemical cross-linking of cellulose

Chemical cross-links are particularly interesting for cellulose as the hydroxyl groups at the C2, C3 and C6 carbons can react to form covalent bonds with numerous other molecules. Therefore in this work, phytic acid was cross-linked to cellulose to reinforce the fiber networks. The use of a multi-functional bio-based solutions such as PA promotes progress towards creating sustainable solutions to cellulose challenges in foams.

Phytic acid, a polyphosphate derived from plants, has been used to improve fire-retardancy in cellulose and fabrics by enhancing the charring of the fiber surface, creating a shield against heat and oxygen.[45–47] Its ability to chelate with metal ions and form hydrogen bonds makes it useful in both inorganic and nonhalogenated flame-retardants (FRs); the non-toxic and competitive alternative to highly regulated halogenated FRs. Phytic acid is soluble in water and thus some degree of cross-linking is required to retain it on washable cellulose substrates.[23,48] An efficient methodology to do so is to react phytic acid and fabrics with compounds containing amine groups such as melamine and diacynamide.[45–47] The result is strong covalent bonds which further increase the FR properties due to the presence of nitrogen. However, this method requires the use of toxic compounds to catalyze the reaction. Others have turned to the use of catalysts such as urea[46] and enzymes[49] to promote the covalent linking between PA phosphate groups and substrate hydroxyl groups. It has also been suggested that the electrostatic potential and hydrogen bonding provides sufficient cross-linking stability when formed via layer-by-layer deposition, although washability has not been verified.[48,50]

The approach taken by this work involves a catalyst-free method to cross-link phytic acid with cellulose fibers. It takes inspiration from traditional fabric finishing techniqueswhere citric acid is hot-pressed or cured onto fabrics to impart strength, wrinkle resistance and laundering durability.[21] Hot-pressing, or curing, applies heat around 120 - 180 °C to the fabric surface. This causes dehydration synthesis, a type of condensation reaction, to occur within citric acid molecules. Heat drives the removal of water from the system, causing hydroxyl groups to react and form highly reactive cyclic anhydrides. Cellulose OH groups then attack the cyclic anhydride, forming a covalent bond between citric acid and cel-

lulose. Citric acid possesses three hydroxyl groups, allowing the condensation reaction to occur twice and synthesizing covalent linkages between cellulose fibers.[51] This technique has also been applied to cellulose fiber foams, making citric acid a common bio-based cross-linker for these foams.[52–55] Thus, the cross-linking of phytic acid to cellulose is hypothesized to also occur via condensation reactions at 160 °C. The result is the formation of both oligo-phosphates and the phosphorylation of PA on cellulose. Here, we elucidate the effect curing temperature has on the molecular structures formed between cellulose fibers and phytic acid and the resulting solid foam properties.

2.5 Mechanical behaviour in compression

As a pore or cell in a foam is compressed, it undergoes three distinct deformation behaviours i) bending linear elasticity ii) buckling plateau and iii) densification. These regions are identifiable in a stress-strain graph such as Figure 2.2. The linear elasticity region defines the modulus or stiffness of the material and is controlled by the resistance of the cell wall/fibers to bending. In closed-cell foams, the amount of material enveloping the cell and the compression of trapped air leads to higher moduli compared to open-cell foams.[7] With less porosity or air inclusion, more fibers can contribute to the strength of the material by forming pore walls.[19,20] In an open-cell configuration, fewer fibers are forming structural walls and compression leads to gas being ejected from the pores. The material may retain some mechanical advantage via reduced connectivity, high strain rates and slowed rate of gas evacuation through tight bottleneck pores. Interestingly, hollow fibers have been found to resist bending much better than solid struts in cell walls. For cellulose, preventing the collapse of the lumen during drying, using never-dried pulp, or chemi-thermomechanical pulp are all viable methods to attain this property.[7,19,56]

The second region is the buckling plateau. At higher stresses, fibers begin to buckle, slip, displace and eventually break as the stress reaches critical levels. The principle mechanism of mechanical failure in fiber foams is caused by weak bonds between fibers as opposed to failure of the fibers themselves.[18] Individual fibers will typically pull-out from each other and unravel to dissipate energy.[7] Thus, the orientation of the fibers and how they interact through slipping or

breaking dictates how the material will deform. It also was noted that dangling ends, loops or free fiber segments do not participate in the material response to mechanical stresses.[13,19] Pöhler et al.[15] postulated that shape recovery of the fiber foam depends on the recovery of fibers from buckling and not on bonding properties. Models describing foam mechanical performance as a result of individual fiber and fiber network deformation behavior has been the subject of recent study by several groups.[15,19,20,57] Pöhler et al.[15] gave a summary of these recent advances in failure mechanism modelling and also explained how the models work well until the addition of physical and chemical cross-linkers. In the final region of foam deformation, stresses cause the cell walls to completely buckle, causing the cell walls to touch. In a stress-strain graph, the slope of the line increases drastically, and densification starts to occur.

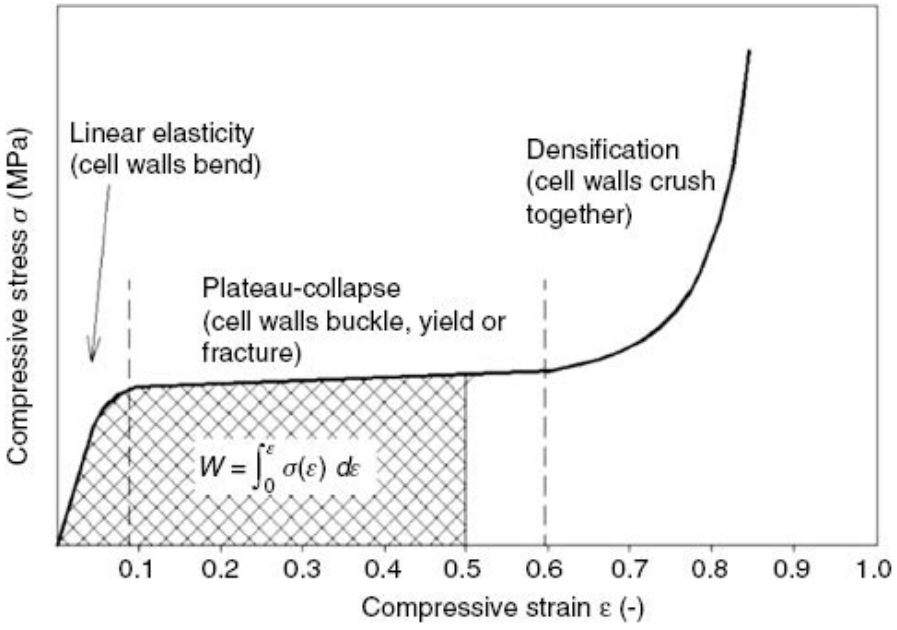

Figure 2.2: Example stress-strain graph of a solid foam mechanical compression test.* Three distinct regions of interest are i) bending linear elasticity, ii) buckling plateau, and iii) densification.

In terms of energy absorption, a foamed material can be optimized to match application-based impact criteria while minimizing density. Specifically, there exists a point where the cell walls are no longer considered elastically buckling and undergo irreversible damage. In polymeric foams, this peak stress is defined by the beginning of the region where densification occurs.[7] The area under

*Credit: Sagar Chandra et al. https://doi.org/10.1515/polyeng-2015-0360

the stress-strain curve up to this point represents the theoretical limit of energy absorption with the possibility of elastic recovery. For a material to be considered reusable in energy absorbing applications, it must be able to absorb all the kinetic energy without damaging the matrix. In a dense foam, the force may exceed the critical damaging value before enough energy has been dissipated through the buckling plateau. On the other hand, low density foams cannot withstand the applied force and will completely collapse, leading to densification before the energy has been absorbed. Thus, the ideal combination of properties would lead to a material with a plateau stress under the critical damaging value and the ability to absorb all the energy before the peak-stress point.[7,30]

3

Experimental

3.1 Preparation of cellulose fiber substrates

3.1.1 Cellulose papers

Whatman Cytiva qualitative filter paper (Grade 5, 47 mm) was purchased from Fisher Scientific. Phytic acid solution (50 % w/w in H_2O) was purchase from Sigma-Aldrich. All reagents purchased were used without further purification. 0.013 mL 50% (w/w) phytic acid solution was diluted in 0.3 mL DI water. The diluted solution was evenly spread over Whatman Cytiva grade 5 qualitative filter paper (0.166 g) without excess, leading to a theoretical dry concentration of 5 wt% phytic acid on dried filters. Filters labelled with a W were washed after curing by adding 200 mL DI water, followed by 100 mL 95% ethanol, and once again with 200 mL DI water in a Büchner funnel. The filters were dried again at 80 °C for 1 hour.

3.1.2 Cellulose foams

Bleached hardwood and softwood kraft pulp fibers were kindly donated by Stora Enso and Pöls, respectively. Hardwood fibers were fibrillated to a Schopper-Riegler (SR) value of 25°. Fibers were dispersed in H_2O to obtain a solid consistency of approximately 15%. Sodium dodecyl sulfate (SDS), carboxymethyl cellulose (CMC) and the cross-linker were added to 3:1 softwood to hardwood fibers obtaining a dry foam composition of 5 wt% CMC, 0.7 wt% SDS and 5 wt% acid cross-linker. The wet ingredients were whipped using a hand-mixer for approximately 30 seconds to achieve a consistent air content. The wet foams were placed in a teflon mold and oven dried.

3.1.3 Oven-drying and curing

Cellulose filters and foams were dried at 80 °C for 15 hours in a convection oven. Post-drying curing conditions and sample nomenclature is provided in Table 3.1. Curing time and temperature were chosen to mimic conditions used by other authors.[21,22,52–55,58,59]

Table 3.1: Nomenclature of cellulose substrates based on curing conditions.

Post drying curing		**Nomenclature***		
Temp.	Time	Control	Citric acid	Phytic acid
20	2 days	20	C20	P20
80	2 hours	80	C80	P80
120	2 hours	120	C120	P120
160	5 mins	160	C160	P160

3.2 Analysis of cellulose fiber substrates

3.2.1 Nuclear Magnetic Resonance (NMR) Spectroscopy

Solid state NMR spectroscopy was performed in a 4 mm ZrO2 MAS rotor with a set temperature of 298K in all experiments. The following parameters were set for ^{13}C and ^{31}P solid state NMR:

^{13}C CP at 10KHz with P3(1H)=3.0us, P15(contact time)=1.5ms, CP at 60.0 kHz 13C (PLW1=109W) SPW0=110W optimized ramp 45-90kHz 1H and 1H decoupling SPINAL64 at 83 kHz (PCPD2=6.0us, PLW12=96W), d1(recovery delay)=2.0s, ns=4000.

^{31}P hpdec at 12.5kHz with P1(31P)=3.5us @PLW1=176W, 1H decoupling TPPM15 at 54 kHz (PCPD2=9.3us, PLW12=40W), d1(recovery delay)=10.0s, ns =64.

*Substrates which appear with a U or W label denote unwashed and washed cellulose filters respectively.

3.2.2 Fourier Transform Infrared (FTIR) Spectroscopy

FTIR was performed on dried cellulose substrates using an attenuated total reflection (ATR) component. Substrates were cured as described by Table 3.1, put immediately in a desiccator, and analyzed soon after, taking the most representative line. A PerkinElmer Fronteir FT-IR spectrometer with PIKE technologies GladiATR was used to measure 32 scans of each substrate 3 times with a data interval of 1 cm^{-1} and 4 cm^{-1} resolution. The scanned wavenumbers were from 400 - 4000 cm^{-1}. PerkinElmer Spectrum software was used to correct for background noise.

3.2.3 Elemental analysis

To determine the phosphorous content on cellulose substrates, elemental analysis was performed by MIKROLAB Mikroanalytisches Laboratorium Kolbe.

3.2.4 Thermogravimetric Analysis (TGA)

In order to understand the degradation behaviour of phosphorylated cellulose papers when exposed to heat, a Mettler Toledo TGA/DSC 3+ was utilized to sequence the following heating sequence using STARe Software: 1. Ramp from 30 °C - 500 °C at a rate of 10 K/min under 60 mL/min air flow, 2. Temperature hold at 500 °C for 5 mins, 3. Ramp from 500 °C - 700 °C at a rate of 10 K/min under 60 mL/min air flow, 4. Temperature hold at 800 °C for 10 mins.

Property values relevant to material flame-retardancy were taken as the average of 3 separately prepared samples. Carbonization onset was set as the point where the initial slope of the graph deviated by more than 3%. Weight loss during carbonization was calculated from this point to where the slope begins levelling out as indicated by a change in slope of 30%. Finally, residual weight was taken as the weight percent of the material remaining at 700 °C.

3.2.5 Determination of density and porosity

The envelope density (ρ_E) of solid foams was measured using calipers and a high-precision balance. Skeletal density (ρ_S) was measured using a Micromeritics AccuPyc II gas displacement pycnometer set with helium gas. Relative density (ρ_R) was given as the ratio of the envelope density to the skeletal density (Equation 3.1). Porosity was then calculated using Equation 3.2.[7]

$$\rho_R = \frac{\rho_E}{\rho_S} \tag{3.1}$$

$$P(\%) = (1 - \rho_R) \cdot 100 \tag{3.2}$$

3.2.6 Mechanical compression testing of fiber foams

To evaluate the mechanical behaviour of the cross-linked cellulose fiber foams, quasi-static compression testing was undertaken in an Instron 5565A Mechanical tester using Bluehill 2 software. A pre-load force of 5N was applied with a 5 kN load cell. The crosshead was lowered at a rate of 5 mm/min until the material reached 60% strain.

The compressive modulus was taken as the slope of the stress-strain curve below 10% strain, while the compressive strength corresponded to the stress at 10% strain. Energy absorption was calculated using the area under the stress-strain curve until up to 50% strain. Variations in density between solid foams were accounted for by dividing all values by their relative density.

3.3 Preparation of CNC suspensions and foams

3.3.1 CNC suspensions

Suspensions were prepared from a 10 wt% CNC stock solution in MilliQ-water and stirred in an IKA EUROESTAR 60 (Germany) overhead stirrer with a four-bladed R-1342 propeller at 1200 rpm for 1 hr. The composition of ternary suspensions consisting of water, TBA, and CNC were designed using JMP Pro 16.2.0 software from SAS (USA). Figure 3.1 summarizes the tested composition range

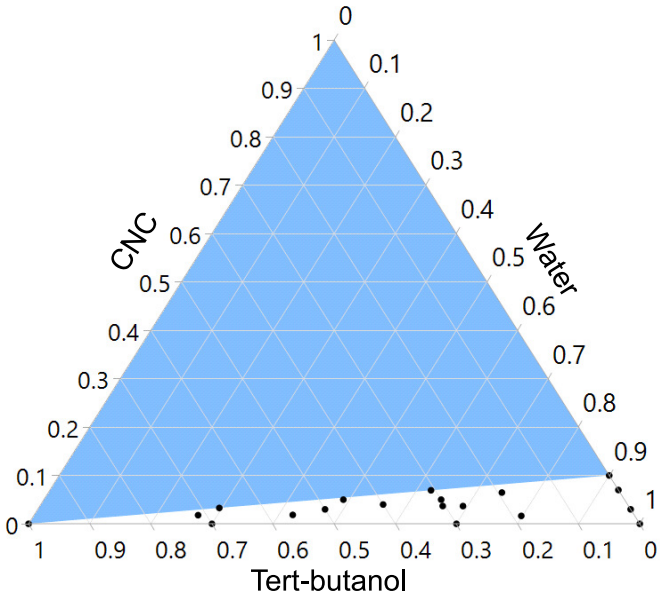

Figure 3.1: Ternary plot summarizing the combinations of suspensions containing concentrations of CNCs, water, and TBA assessed in this study (black dots).

(white region) as the actual range was limited to 10 wt% CNCs in water. The suspensions were then prepared by diluting the stock suspension in water and TBA was added in seven incremental steps to avoid heterogeneous or phase-separated suspension, with thorough shaking after each step. Finally, the suspensions were shaken overnight on a moving platform at 180 rpm.

3.3.2 Freeze-drying

To transform the suspensions into free-standing dry foams, they were first injected into molds and degassed. The molds were subsequently submerged in liquid nitrogen and placed in a ScanVac CoolSafe freeze-dryer at -105 °C for 2 days. The solid foams are believed to maintain an intact structure when subjected to rapid freezing followed by freeze-drying.[60]

3.4 Analysis of CNC foams

3.4.1 Brunauer-Emmett-Teller (BET) surface area

The surface area was determined using a Micrometrics TriStar 3000 with TriStar II Plus software and N_2 gas at 0-0.98 relative pressure. For BET linearization, the relative pressure corresponding to the nitrogen monolayer coefficient in the BET equation was included and the maximum value of the Rouquerol BET graph was the last chosen point.

3.4.2 Scanning electron microscopy (SEM)

The solid foams were cut through the center and sputter-coated with 4 nm of gold. A JEOL 7800F Prime instrument was used to visualize the coated surface at an acceleration voltage of 5 kV.

3.4.3 Mechanical compression testing of CNC foams

Solid foams were conditioned at 20 °C in a desiccator for a week before mechanical testing. Compression tests were performed using a Texture Analyser (Stable Microsystems, UK) with a crosshead rate of 1 mm s^{-1} after reaching a pre-load force of 0.5 N. The solid foams were pressed between parallel plates of 40 mm in diameter using a load cell of 50 kg.

4

Results and Discussion

In the interest of strengthening the structure of cellulose foams, approaches towards chemical cross-linking and pore structure formation were evaluated. Phosphorylation of cellulose with a polyphosphate such as phytic acid was hypothesized to form covalent bonds between cellulose fibers. This would strengthen fiber-fiber contacts and provide flame-retardancy to the cellulose foam. On the other hand, using a structuring co-solvent such as TBA was hypothesized to create a template around which cellulose can assemble. By understanding the liquid-phase structuring of TBA in water and its interactions with CNCs, control over the pore formation when developing the solid foams could be achieved. To investigate these ideas, mechanical compression testing was used to reveal changes in the modulus, strength and energy absorption of the solid foams. Then, analysis of the key underlying structures using techniques such as FTIR and NMR for molecular changes, and SEM to visualize morphological changes was performed.

4.1 Cellulose cross-linking via phytic acid

4.1.1 Dehydration synthesis condensation reactions

Hydroxyl-rich phosphates from PA come into contact with both cellulose and other PA molecules when spread on the surface of the cellulose substrates. When hot-pressing or curing is applied, a covalent cross-link between these molecules is proposed to have formed as heat drives the removal of water.[58] Figure 4.1 displays the mechanisms and products which may arise due to the dehydration synthesis between cellulose and phytic acid.[61] Each mechanism depends on the environment and reactivity of nearby molecules.

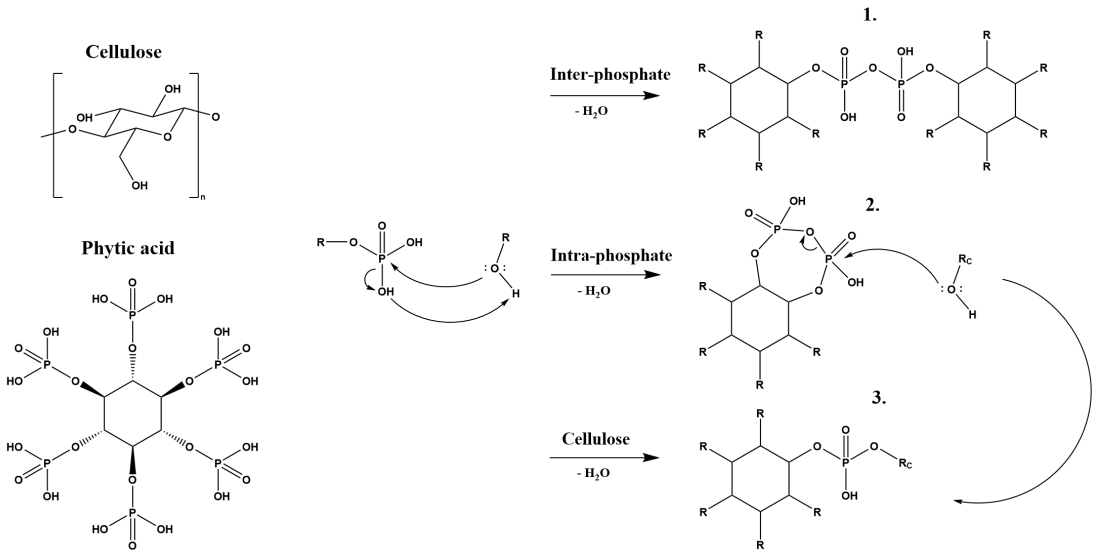

Figure 4.1: Molecular structures of cellulose and phytic acid with proposed mechanisms for dehydration synthesis condensation reactions between them. The reactants comprise of a phosphate group and either cellulose or another phytic acid molecule where R is either phosphate groups (PO_3H^-) or C2, C3 or C6 of cellulose. R_C is defined specifically as C2, C3 or C6 of cellulose. Products 1, 2 and 3 are the proposed products of the reaction, depending on the mechanism of action described above the reaction arrow. Product 2 may react rapidly with cellulose generating product 3 as indicated by the curved arrow.

The electrophilicity of phosphorus in phosphate groups encourages nucleophilic attack by both cellulose and other phosphate groups. The hydroxyl groups of attacking phosphates are more nucleophilic than cellulose OH groups due to the lower electronegativity of the phosphorus group.[61,62] Thus, inter-phosphorylation reactions between PA molecules are favored and generate product 1, a mechanism which is well supported in literature.[45,48,62] This reaction may propagate, creating large oligo-phosphate chains with sufficient nearby phosphates. However, the low concentration of phytic acid distributed on the surface of the cellulose substrates in this study suggests two competing reactions. In a dilute system of phosphates, cellulose is hypothesized to undergo phosphorylation, generating product 3. An intra-phosphorylation reaction may generate a reactive cyclic anhydride shown in product 2; similar to the product made when curing citric acid. The structure would be susceptible to nucleophilic attack by cellulose, thereby creating product 3 as shown by the curved arrow.

When phytic acid undergoes dehydration synthesis, the phosphates change from being monoesters to diesters. We can visualize this by tracking the shift of the monoester band at 1250 cm^{-1} to lower wavenumbers (1250-1210 cm^{-1}) for diesters.[63] In our system, we see a shift in the band from 1249 cm^{-1} (P20U) to 1243 cm^{-1} (P160W) (Figure 4.2). The displacement of the band depends on the nature of the element forming the diester bond, and the excess of unreacted phosphates.

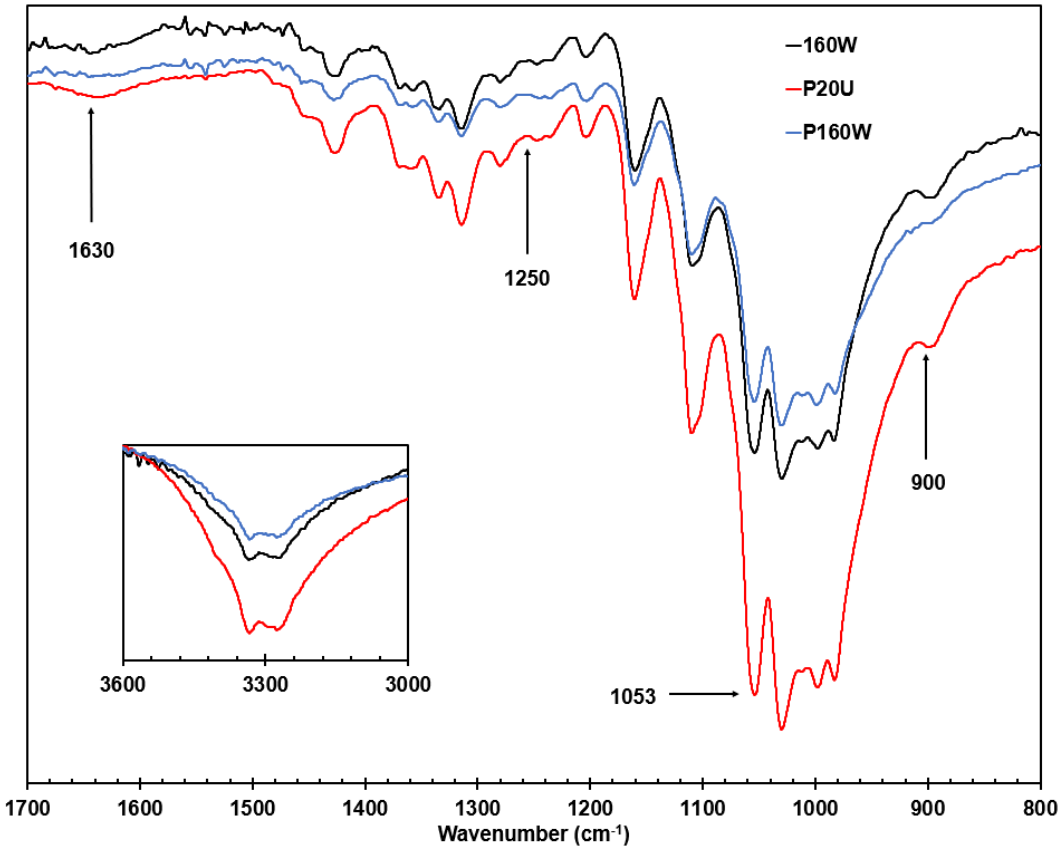

Figure 4.2: FTIR spectrum comparing a blank cellulose substrate exposed to 160 °C curing and washed (160W), a substrate cured with phytic acid at 160 °C and washed (P160W), and a substrate with phytic acid and dried at RT (P20U).

The successful synthesis reactions to form product 3 can be verified by evaluating the intensity of FTIR bands at 1630 and 3300 cm^{-1}. The band at 1630 cm^{-1} represents water bound to cellulose and phytic acid via hydrogen bonding while 3300 cm^{-1} describes the hydroxyl groups present on both cellulose and phytic acid. Therefore, the band intensity at 3300 cm^{-1} was expectedly highest for the cellulose substrate coated in phytic acid dried at room temper-

ature (P20U). This in turn also maximized the capacity for hydrogen bonding, increasing the intensity of the peak at 1630 cm^{-1}. When the substrate was cured by heating it at 160 °C, bound water was evaporated, reducing this peak as seen in both cellulose and cellulose with phytic acid (160W and P160W). The intensity at 3300 cm^{-1} for P160W decreases below that of the substrate without PA (160W), giving an indication that dehydration synthesis reactions with cellulose hydroxyl groups have occurred and covalent ester bonds were formed. This can be further supported by observing the increase in ratio between the peak at 1053 cm^{-1} (δ_{C-O-P}) and 900 cm^{-1} (δ_{P-O-P}) for P20U and P160W.[58,63] As the ratio rises from 0.96 to 0.98 respectively, ester bonds to carbon are formed.

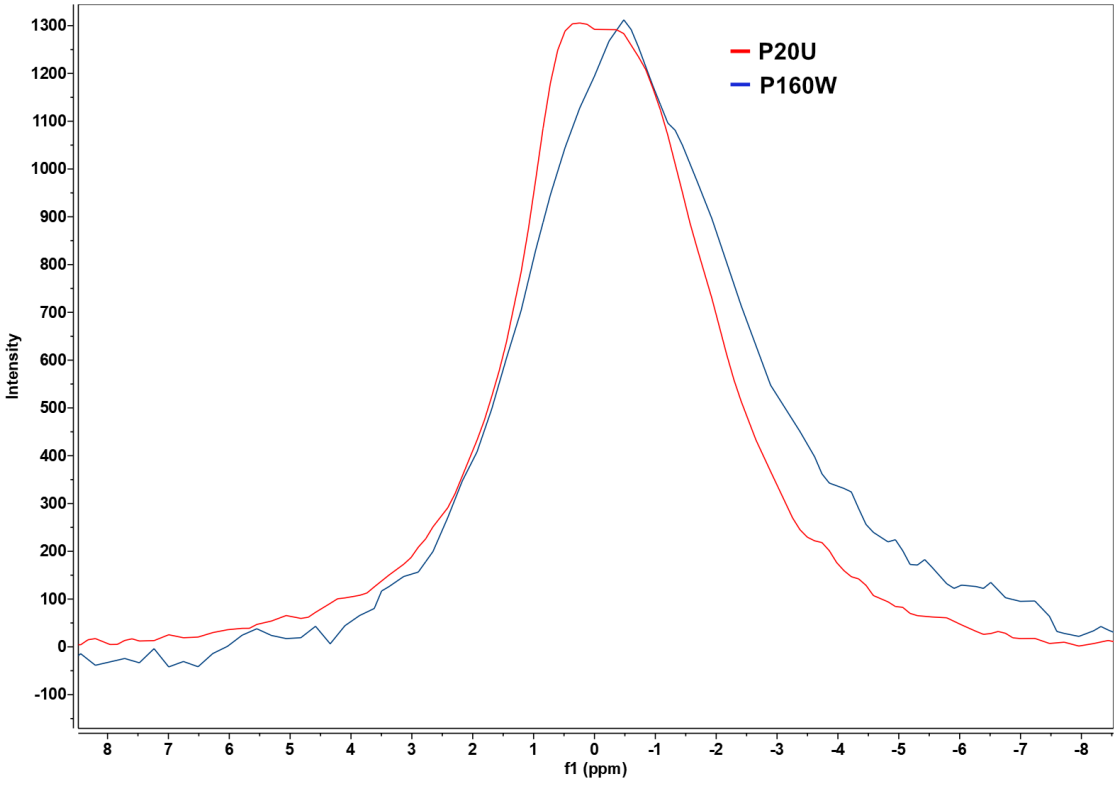

Figure 4.3: Stacked ^{31}P solid state NMR peaks depicting a peak intensity shift from -0.45 ppm (P20U) to 0.24 ppm (P160W) after curing. Peaks were re-scaled to similar intensities for comparison.

This effect can also be visualized in the solid state ^{31}P-NMR spectrum (Figure 4.3). As the OH group on the phosphate changes to a covalent ester bond with either C or another P, a shift to the right in the primary phosphorus peak is expected as the phosphorus becomes more deshielded. However, NMR results provide no indication of whether the ester linkage is to hydroxyls attached to

carbon or another phosphate group. Rather, it provides substantial evidence that PA phosphates change from mono to diester linkages and therefore the presence of product 1 is still likely and should not be discounted.

Separate analysis of these signals revealed a gradual increase in the phosphorus peak intensity of washed substrates cured at higher temperatures. This result was confirmed by the increased phorsphorous content seen in elemental analysis (Table 4.1). The decrease in phosphorus content from the washing step was noticeably minimized on substrates treated with progressively high curing temperatures. Notably, P20W substrates retained very little phosphorus, indicating that hydrogen bonding between phosphate and cellulosic hydroxyl groups was insufficient to retain PA on the fiber surfaces. Therefore, phosphorylation likely created covalently bound PA molecules which were increasingly difficult to remove from the cellulose matrix when cured at higher temperatures. While covalent bonds to cellulose are proposed as the primary product of this reaction, the formation of inter-phosphorylated PA chains may create large structures which have reduced solubility in water and ethanol, and are physical restrained within the cellulose network due to entanglements and frictional forces. This would also potentially allow phosphorus to be retained in the cellulose substrates without covalently binding it to cellulose molecules.

Table 4.1: Phosphorus content (weight %) on cellulose substrates treated with PA detected via elemental analysis.

Substrate	**Unwashed**	**Washed**
P20	1.78	0.05
P80	1.66	0.08
P120	1.65	0.27
P160	1.42	0.70

4.1.2 Substrate properties

The addition of phytic acid to cellulose fibres caused changes in crystallinity. Crystalline domains of cellulose at C4 and C6 are indicated by broad peaks at 63 and 84 ppm in solid state ^{13}C-NMR (Figure 4.4).[64] The addition of PA to the cellulose substrates caused both of these peaks to decrease in intensity, with curing at 160 °C decreasing intensity even further. The degradation of PA to gaseous phosphoric acids at 160 °C likely degraded the crystalline moieties further.[65] Reduction in cellulose crystallinity would cause a weakening of the cellulose fibre structure, creating a network with worse mechanical performance. However, successful phosphorylation of cellulose would indicate that covalent cross-links between fibers is possible, which would lead to improved mechanical strength. Therefore, competition between these effects was expected to cause visible changes on the mechanical properties of the cellulose fiber foams.

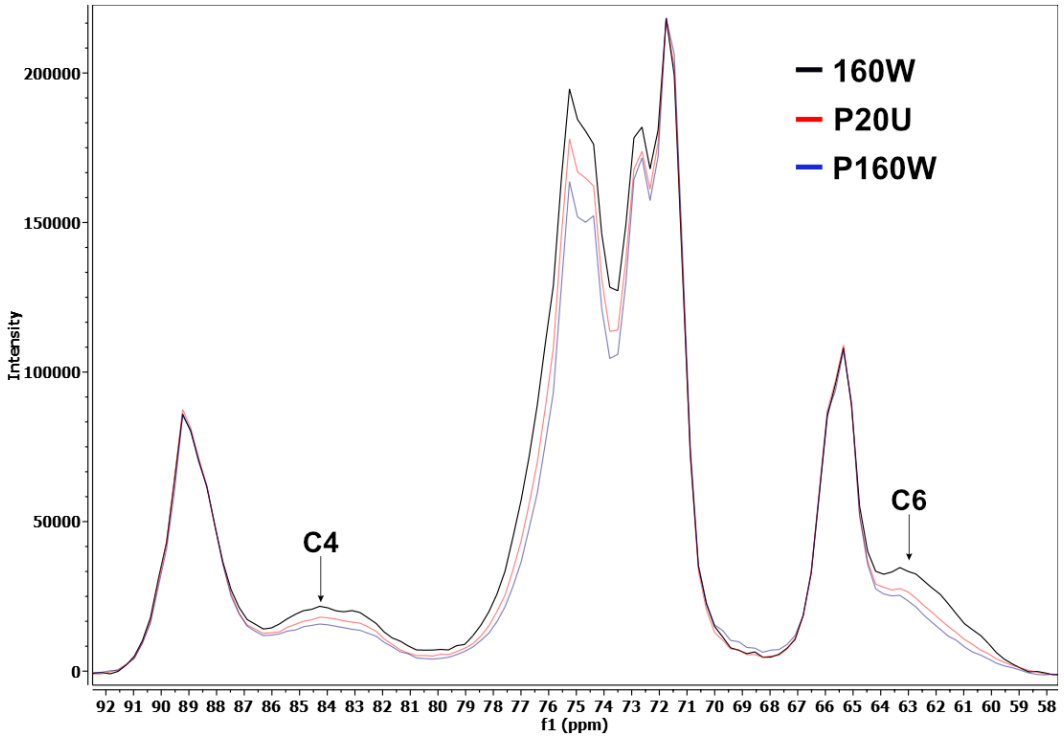

Figure 4.4: Solid state ^{13}C-NMR of cellulose substrates comparing the effect of PA and curing on cellulose surface C4 and C6 moietites. Cured blank cellulose substrate (160W), PA on cellulose substrate (P20U), and a cellulose substrate cured with PA (P160W) were auto-scaled to match interior moieties of C4 and C6 at 66 and 89 ppm.

To verify how phytic acid affected the fiber network, compression testing of cellulose fiber foams cured at different temperatures was performed. The results were compared against foams similarly cured with citric acid and foams without any cross-linker added. The cellulose substrates displayed a progressive visual darkening at each higher curing temperature as shown in Figure 4.5i. In terms of mechanical performance, P80 had significantly lower properties when compared to the control foam (80) (Figure 4.5ii,iii,iv). At this curing temperature, it was thus concluded that degradation of crystalline cellulose domains is the dominant mechanism governing performance. P120 had improved mechanical properties when compared to P80, yet did not outperform the control. However, P160 demonstrated a significant improvement in both modulus and strength. In terms of modulus P160 even outperformed C160, the citric acid cross-linking, matched it in strength. Where P160 suffered however was in energy absorption, likely due to the observably brittle structure. Phosphorylation of cellulose using phytic acid therefore successfully forms covalent bonds between fibers, creating mechanically strong fiber networks.

The flame-retardancy mechanism of organophosphates and phytic acid is well understood. In general, the thermal stability of phytic acid is low in comparison to cellulose and other materials due to the hygroscopicity of the multiple phosphate groups. As temperature increases, the molecule begins to decompose, forming phosphoric acids. These acids catalyse the dehydration of cellulose, causing the onset of carbonization. As the accelerated carbonization of cellulose occurs, a char layer is formed on the surface of the fibers. This char creates a physical barrier against heat and oxygen, which prevents further degradation of the fibers.[23]

According to a study by Daneluti and Matos,[65] the onset of phytic acid carbonization was determined to be around 160 °C for pure phytic acid when analysed via thermogravimetric analysis (TGA). They also noted a visual darkening of the solution when the solution was treated at 150 °C, which they ascribed to carbonization of the phytic acid. We suggest that this carbonization reaction occurs gradually with temperature increase as the cellulose substrates displayed a progressive visual darkening at each higher curing temperature (Figure 4.5i) and TGA curves changed significantly (Figure 4.6a). Unwashed substrates with PA gradually rose in carbonization onset with increasing curing temperature as

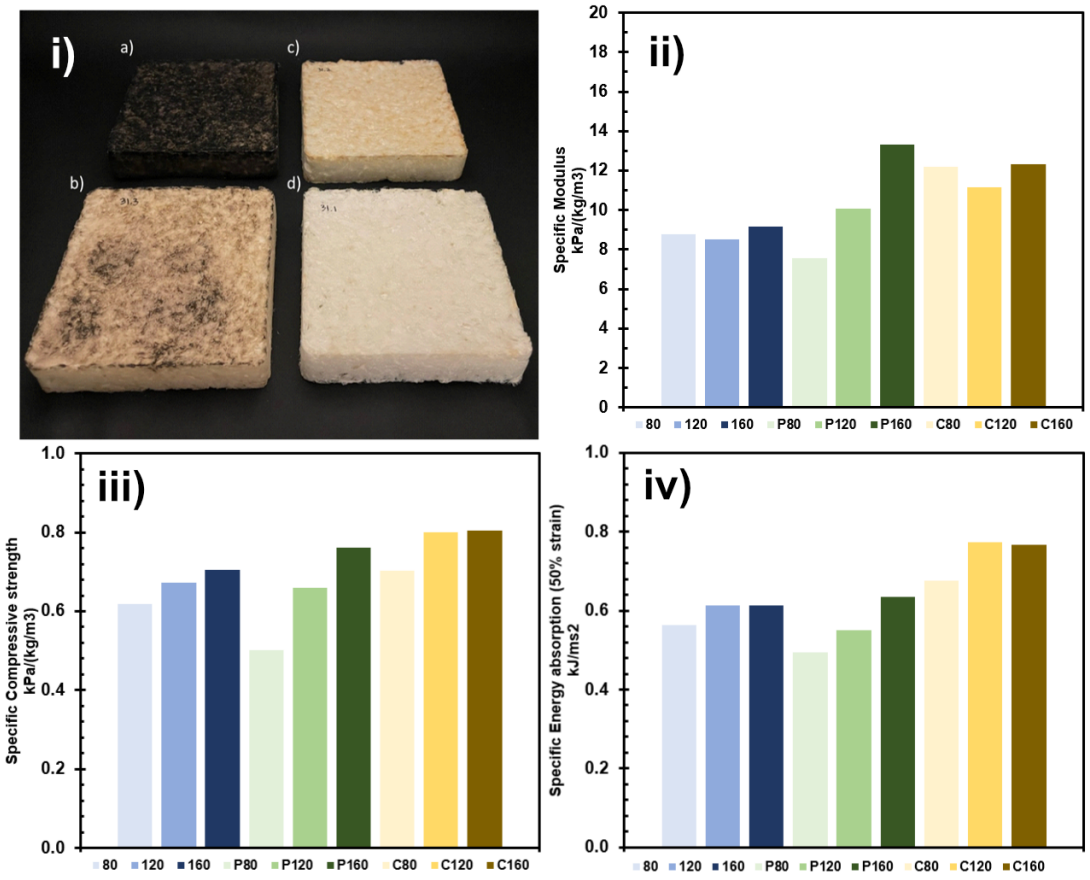

Figure 4.5: Cellulose fiber foams showing i) visual darkening with higher curing temperatures for a) P160, b) P80, c) C160 and d) 160, and bar graphs of specific compressive properties ii) modulus, iii) strength, and iv) energy absorption. The bar graph legend describes the crosslinker used (P = PA, C = CA) and the temperature at which the foam was cured.

shown in Figure 4.6b. This indicates a reduction in the initial ability of the material to cause carbonization, which correlates well with the phosphorus content found in elemental analysis. However, the interesting finding was the material properties after washing. As curing temperature increased, the change in property values from unwashed substrates was incrementally minimized (Figure 4.6). P160W in particular changed by less than 5% in all evaluations. However this result lacks consistency when compared to the reduction of nearly 50% in phosphorus content found by elemental analysis in Table 4.1.

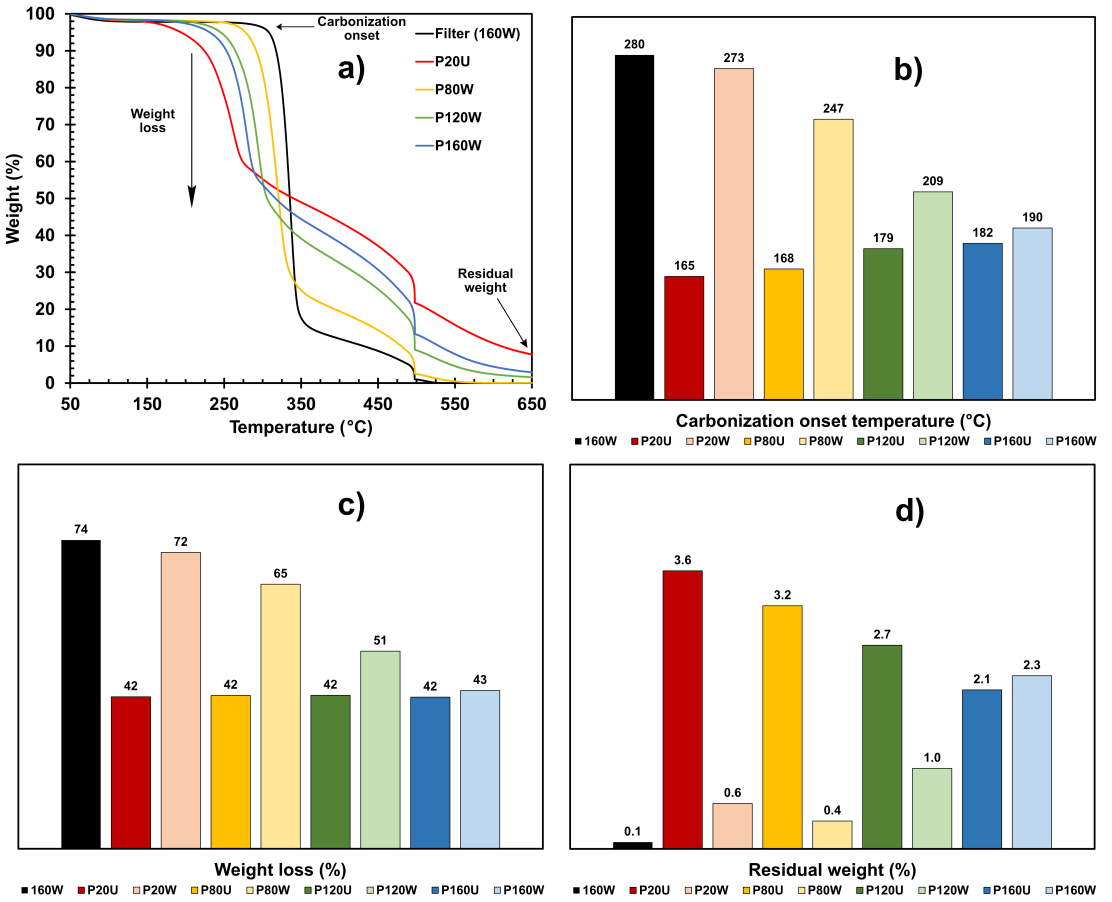

Figure 4.6: TGA analysis of cellulose filters with phytic acid showing a) the full TGA graph with points of analysis, b) carbonization onset temperature, c) weight loss in percent due to carbonization and d) residual weight in percent at 800°C. The number following P is the curing temperature while U and W are unwashed and washed substrates respectively.

4.2 Hierarchical structuring via TBA templating

To evaluate the effect a structuring agent such as TBA has on a cellulose network, CNCs were instantly frozen in liquid nitrogen and freeze-dried to maintain the structuring present in the liquid-phase. Foams from CNC-water suspensions displayed layered sheet-like lamellar macro-structures (Figure 4.7a). Upon closer inspection, the sheet micro-structure reveals homogenous surfaces, indicating a highly densified packed structure of CNCs. This showcases how CNCs form networks which have high short-range interactions between crystals yet poor macro-connectivity throughout the foam. The disparate nature of the structures

caused these foams to display poor mechanical performance in comparison to other tested foams. Increasing the concentration of CNCs reinforced the sheets, improving mechanical properties at the cost of reduced porosity (Table 4.2). Interestingly, the surface area of foams above 4 wt% CNCs was consistently below 5 m^2/g, and increased drastically to 15 m^2/g at 3 wt% CNC concentration.

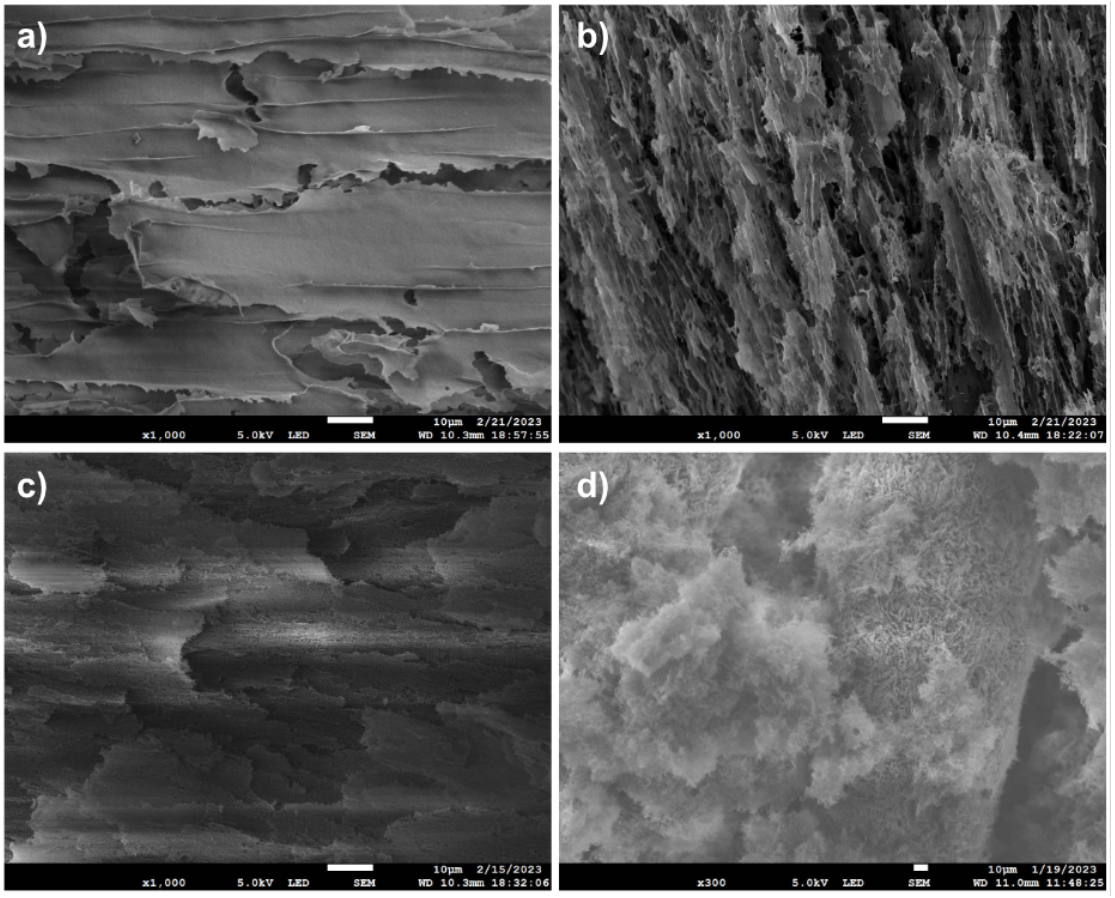

Figure 4.7: SEM images of representative structures found in CNC foams at 1000x magnification. The TBA content and morphology description are given as a) 0 wt% TBA (lamellar, paper), b) 30-50 wt% TBA (tubular, algae), c) <30 wt% TBA (porous lamellar), and d) >60 wt% TBA (fibrillated, mossy).

To improve the hierarchical network of the CNC foams, TBA was introduced as a templating agent. At similar concentrations of CNCs, the addition of any TBA immediately strengthened the foam structure and created high surface areas. The trend in property values indicated that using TBA could compensate mechanically for lower CNC concentrations. For example, the specific moduli of 7 wt% and 10 wt% CNC foams without TBA were 22 and 40 MPa respectively; whereas that of 4 wt% CNC with addition of 40% TBA exhibited a modulus of

36 MPa (Table 4.2). Solid foams with 7 wt% CNCs demonstrated clearly how the presence of TBA altered the morphology of the CNC network. The lamellar sheets of 7CNC0T (Figure 4.7a) were transformed into algae-like structures with a more macro-structurally homogeneous texture in 7CNC30T (Figure 4.7b). The formation of disrupted tube-like structures seemed to ameliorate connectivity throughout the 7CNC30T foam. As a result of this changed morphology, the strength and stiffness of 7CNC30T increased by 180%, energy absorption by 120%, and surface area rose from 5 m^2/g to 52 m^2/g compared to 7CNC0T (Table 4.2). The bicontinuous nature of the suspension at this TBA concentration was concluded to have altered the assembly of CNC structures to shape around TBA-rich regions.[25]

Table 4.2: Experimental values for surface area, specific modulus, specific energy absorption, and specific compressive strength of solid foams obtained from the suspensions denoted in the first column. Foams are labelled xCNCyT where x and y represent the wt% of CNCs and TBA respectively in the suspensions.

	Surface Area (m^2/g)	**Modulus (MPa)**	**Energy Abs. (MJ/m^3)**	**Strength (MPa)**
4CNC30T	71	9.0	0.83	1.1
4CNC40T	56	36	2.45	1.5
6CNC19T	80	21	1.67	1.7
7CNC0T	4.9	22	1.58	1.4
7CNC30T	52	64	4.32	3.0
10CNC0T	4.0	40	3.15	1.7

This result could be confirmed by observing the morphology of a foam formed from 6 wt% CNCs and 19 wt% TBA in Figure 4.7c. The formation of small micropores within the lamellar sheets indicated that CNCs had assembled around small TBA-rich regions, generating the peak surface area of all the solid foams. High (>60 wt%) TBA concentrations displayed similar surface areas yet had vastly different morphologies. Figure 4.7d shows the formation of large aggregated porous structures with dispersed "mossy" formations on their surface. Large TBA-rich regions formed disparate structures, which had poor compressive mechanical performance and phase separated as suspensions.

An indirect relationship between mechanical properties and surface area was apparent for systems containing TBA as a co-dispersant (Figure 4.8). At low (<30 wt%) and high (>60 wt%) concentrations of TBA, surface area was maximized yet mechanical properties were mostly unchanged compared to solid foams with 0% TBA. On the other hand, incorporation of 30-50 wt% TBA in CNC suspensions resulted in outstanding compressive mechanical performance. Therefore, solid foams in this range can be tailored towards applications requiring high specific mechanical performance while maintaining a greater surface area than foams devoid of TBA.

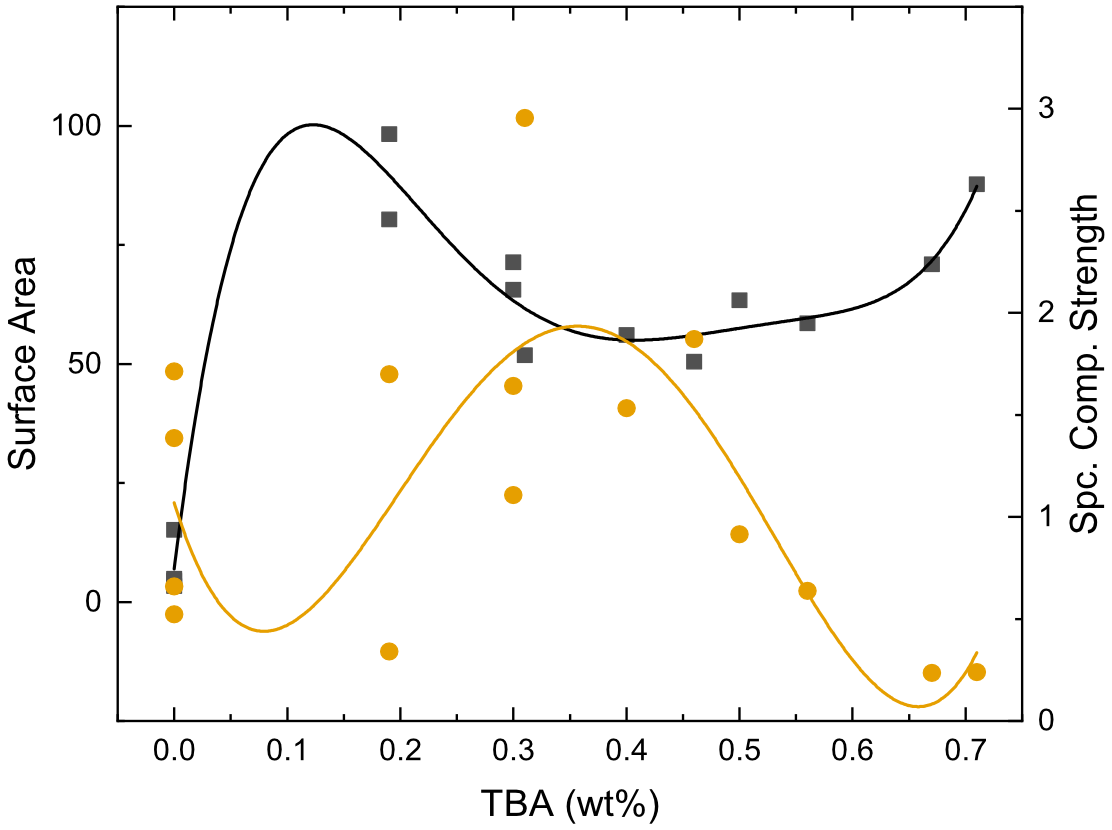

Figure 4.8: The inverse correlation between surface area and specific compressive strength in CNC foams with changing TBA wt%. Surface area is shown in black and compressive strength in yellow.

5

Conclusions

By drawing inspiration from the hierarchical structures in nature, the goal of this thesis work was to present solutions to a challenge faced when working with cellulose substrates: strengthening of cellulose fiber foams. Phytic acid (PA) is a multifunctional bio-based component which enables solutions towards forming mechanically performant cellulose fiber foams that are fire-retardant. In systems with dilute concentrations of PA, the proposed dehydration synthesis reaction initiated via curing with heat was confirmed, indicating the successful phosphorylation of cellulose. This provides a catalyst-free methodology to cross-link PA with cellulose. Knowledge of the reaction mechanisms and conditions allows this phosphate cross-linking technology to be applied in strengthening cellulose fiber materials such as foams. The concept can also be adapted toward other hydroxyl containing substrates.

To structure pore formation in cellulose foams a tertiary alcohol, TBA, was employed as a co-solvent in aqueous cellulose systems and was shown to direct the assembly of CNCs. TBA inhibited CNC packing into highly densified lamellar sheets, instead forming hierarchical cellular structures in the dried foams. Control over the TBA concentration changed the assembly, allowed modulation of the mechanical performance and surface area. This templating method demonstrates how co-solvents may be used in cellulose systems to create foams with tuned pore structures.

6

Outlook

Overcoming obstacles is rooted in the human ability to survive. In the face of the mounting climate crisis, it is time for our generation to turn to solutions which can reduce our energy consumption and production of greenhouse gasses. To that end, this work showcases cellulose substrates and lightweight construction as two facets which represent major players in the materials industry. In an effort to guide and inspire future works, important considerations and solutions to fundamental issues are outlined in the use of cellulose for lightweight materials.

The successful phosphorylation of cellulose using curing technologies marks an important transition to using non-toxic bio-based compounds for flame retardant materials. Phytic acid cross-linking provides solutions to two major issues which plagues the development of cellulose: strength of fiber networks and fire-resistance. This bio-based molecule also provides multifunctionality, a trait which is becoming increasingly valuable in the materials world. The established concept can now be considered for applications in materials manufacturing and what limitations regarding the materials performance remain.

The porous network structure necessary for lightweight materials also governs an important part of material behavior. Finding adaptable solutions to control the formation of this structure, such as use of co-solvents, is therefore crucial when designing the material for specific functions. Strengthening by combination of chemical and physical means is going to be a necessary part of the solution. The concepts provided in this work are not necessarily limited to cellulose, and should be used to inspire the advancement of bio-based lightweight materials as promising alternatives for structural materials.

Bibliography

[1] R. Lakes, *Nature*, 1993, **361**(6412), 511–515.

[2] F. J. Martin-Martinez, K. Jin, D. Lopez Barreiro, and M. J. Buehler, *ACS Nano*, 2018, **12**(8), 7425–7433.

[3] M. A. Meyers, J. McKittrick, and P.-Y. Chen, *Science*, 2013, **339**(6121), 773–779.

[4] U. G. Wegst, H. Bai, E. Saiz, A. P. Tomsia, and R. O. Ritchie, *Nature Materials*, 2015, **14**(1), 23–36.

[5] M. Rinaudo, *Progress in Polymer Science*, 2006, **31**(7), 603–632.

[6] M. A. Meyers, P.-Y. Chen, M. I. Lopez, Y. Seki, and A. Y. Lin, *Journal of the Mechanical Behavior of Biomedical Materials*, 2011, **4**(5), 626–657.

[7] M. F. Ashby and L. J. Gibson, *Cellular Solids: Structure and properties*, Cambridge University Press, London, UK, 1997.

[8] M. A. Meyers and P.-Y. Chen, *Biological Materials Science: Biological materials, Bioinspired materials and biomaterials*, Cambridge University Press, London, UK, 2014.

[9] M. C. Fernandes, J. Aizenberg, J. C. Weaver, and K. Bertoldi, *Nature Materials*, 2021, **20**(2), 237–241.

[10] Y. Bienvenu, *Comptes Rendus Physique*, 2014, **15**(8), 719–730.

[11] J. Njuguna, *Lightweight Composite Structures in Transport: Design, Manufacturing, Analysis and Performance*, Woodhead Publishing, 2016.

[12] T. Aziz, A. Farid, F. Haq, M. Kiran, A. Ullah, K. Zhang, C. Li, S. Ghazanfar, H. Sun, R. Ullah, A. Ali, M. Muzammal, et al., *Polymers*, 2022, **14**(15).

[13] R. Sescousse, R. Gavillon, and T. Budtova, *Carbohydrate Polymers*, 2011, **83**(4), 1766–1774.

[14] T. Pöhler, P. Jetsu, A. Fougerón, and V. Barraud, *Nordic Pulp & Paper Research Journal*, 2017, **32**(3), 367–374.

[15] T. Pöhler, J. A. Ketoja, T. Lappalainen, V.-M. Luukkainen, I. Nurminen, P. Lahtinen, and K. Torvinen, *Cellulose*, 2020, **27**, 6961–6976.

[16] S. Paunonen, O. Timofeev, K. Torvinen, T. Turpeinen, and J. A. Ketoja, *BioResources*, 2018, **13**(2), 4058–4074.

[17] P. Nechita and S. Năstac, *Journal of Composite Materials*, 2018, **52**(6), 747–754.

[18] A. Madani, S. Zeinoddini, S. Varahmi, H. Turnbull, A. Phillion, J. Olson, and D. Martinez, *Cellulose*, 2014, **21**, 2023–2031.

[19] J. A. Ketoja, S. Paunonen, P. Jetsu, and E. Pääkkönen, *Materials*, 2019, **12**(3), 384.

[20] T. Mäkinen, J. Koivisto, E. Pääkkönen, J. A. Ketoja, and M. J. Alava, *Soft Matter*, 2020, **16**(29), 6819–6825.

[21] C. Q. Yang, X. Wang, and I.-S. Kang, *Textile Research Journal*, 1997, **67**(5), 334–342.

[22] A. D. Štiglic, F. Gürer, F. Lackner, D. Bračič, A. Winter, L. Gradišnik, D. Makuc, R. Kargl, I. Duarte, et al., *iScience*, 2022, **25**(5), 104263.

[23] W. Liu, R. Shi, X. Ge, H. Huang, X. Chen, and M. Mu, *Progress in Organic Coatings*, 2021, **156**, 106271.

[24] X. Xie, T. Yuan, Y. Yao, G. Li, Y. Li, and X. Wang, *Colloids and Surfaces A: Physicochemical and Engineering Aspects*, 2023, **659**, 130749.

[25] T. Buchecker, S. Krickl, R. Winkler, I. Grillo, P. Bauduin, D. Touraud, A. Pfitzner, and W. Kunz, *Physical Chemistry Chemical Physics*, 2017, **19**(3), 1806–1816.

[26] J. Cerar, A. Jamnik, I. Pethes, L. Temleitner, L. Pusztai, and M. Tomšič, *Journal of Colloid and Interface Science*, 2020, **560**, 730–742.

[27] J. J. Bikerman, *Foams*, Springer Berlin, Heidelberg, 2013.

[28] T. Lappalainen and J. Lehmonen, *Nordic Pulp & Paper Research Journal*, 2012, **27**(5), 930–939.

[29] K. Ganesan, A. Barowski, L. Ratke, and B. Milow, *Journal of Sol-Gel Science and Technology*, 2019, **89**, 156–165.

[30] K. Ganesan, A. Dennstedt, A. Barowski, and L. Ratke, *Materials & Design*, 2016, **92**, 345–355.

[31] R. Li, J. Du, Y. Zheng, Y. Wen, X. Zhang, W. Yang, A. Lue, and L. Zhang, *Cellulose*, 2017, **24**, 1417–1426.

[32] H. Malekzadeh, N. Md Zaid, and E. Bele, *Cellulose*, 2021, **28**, 703–714.

[33] J. Lee and Y. Deng, *Soft Matter*, 2011, **7**(13), 6034–6040.

[34] H. Bäckdahl, M. Esguerra, D. Delbro, B. Risberg, and P. Gatenholm, *Journal of Tissue Engineering and Regenerative Medicine*, 2008, **2**(6), 320–330.

[35] N. Pircher, D. Fischhuber, L. Carbajal, C. Strauß, J.-M. Nedelec, C. Kasper, T. Rosenau, and F. Liebner, *Macromolecular Materials and Engineering*, 2015, **300**(9), 911–924.

[36] J. Li, T. Song, H. Xiu, M. Zhang, R. Cheng, Q. Liu, X. Zhang, E. Kozliak, and Y. Ji, *Industrial Crops and Products*, 2018, **125**, 314–322.

[37] A. Borisova, M. De Bruyn, V. L. Budarin, P. S. Shuttleworth, J. R. Dodson, M. L. Segatto, and J. H. Clark, *Macromolecular Rapid Communications*, 2015, **36**(8), 774–779.

[38] M. D. Hands and L. V. Slipchenko, *The Journal of Physical Chemistry B*, 2012, **116**(9), 2775–2786.

[39] M. Kiselev and D. Ivlev, *Journal of Molecular Liquids*, 2004, **110**(1-3), 193–199.

[40] F. Jiang, *Handbook of Fibrous Materials*, 2020, pp. 95–124.

[41] H. Sixta et al., *Handbook of Pulp*, Wiley-VHC Verlag GmbH and Co., 2006.

[42] T. Hjelt, J. A. Ketoja, H. Kiiskinen, A. I. Koponen, and E. Pääkkönen, *Journal of Dispersion Science and Technology*, 2022, **43**(10), 1462–1497.

[43] P. Jahangiri, R. Korehei, S. S. Zeinoddini, A. Madani, Y. Sharma, A. Phillion, D. M. Martinez, and J. A. Olson, *Nordic Pulp & Paper Research Journal*, 2014, **29**(4), 584–591.

[44] O. Korhonen and T. Budtova, *Composites Part A: Applied Science and Manufacturing*, 2020, **137**, 106027.

[45] S. Thota, V. Somisetti, S. Kulkarni, J. Kumar, R. Nagarajan, and R. Mosurkal, *Cellulose*, 2020, **27**, 11–24.

[46] X.-h. Liu, Q.-y. Zhang, B.-w. Cheng, Y.-l. Ren, Y.-g. Zhang, and C. Ding, *Cellulose*, 2018, **25**, 799–811.

[47] H.-B. Yuan, R.-C. Tang, and C.-B. Yu, *International Journal of Molecular Sciences*, 2021, **22**(17), 9631.

[48] F. Song, Q. Zhao, T. Zhu, C. Bo, M. Zhang, L. Hu, X. Zhu, P. Jia, and Y. Zhou, *Materials & Design*, 2022, **221**, 110925.

[49] X.-T. Zheng, Y.-Q. Dong, X.-D. Liu, Y.-L. Xu, and R.-K. Jian, *Journal of Cleaner Production*, 2022, **350**, 131525.

[50] Z. Wang, Z. Ma, S. Wang, M. Pi, X. Wang, M. Li, H. Lu, W. Cui, and R. Ran, *Carbohydrate Polymers*, 2022, **298**, 120128.

[51] Z. Cai, B. Ji, K. Yan, and Q. Zhu, *Polymers*, 2019, **11**(12), 2071.

[52] E. S. Ferreira, E. D. Cranston, and C. A. Rezende, *ACS Sustainable Chemistry & Engineering*, 2020, **8**(22), 8267–8278.

[53] A. Meftahi, R. Khajavi, A. Rashidi, M. Rahimi, and A. Bahador, *Journal of Nanostructure in Chemistry*, 2018, **8**, 311–320.

[54] A. Ottenhall, T. Seppänen, and M. Ek, *Cellulose*, 2018, **25**(4), 2599–2613.

[55] A. N. Frone, D. M. Panaitescu, C. A. Nicolae, A. R. Gabor, R. Trusca, A. Casarica, P. O. Stanescu, D. D. Baciu, and A. Salageanu, *Materials Science and Engineering: C*, 2020, **110**, 110740.

[56] A. Tejado, W. C. Chen, M. N. Alam, and T. G. van de Ven, *Cellulose*, 2014, **21**, 1735–1743.

[57] P. Bergström, S. Hossain, and T. Uesaka, *International Journal of Solids and Structures*, 2019, **166**, 68–74.

[58] Q. Guo, J. Cao, Y. Han, Y. Tang, X. Zhang, and C. Lu, *Green Chemistry*, 2017, **19**(14), 3418–3427.

[59] C. Demitri, R. Del Sole, F. Scalera, A. Sannino, G. Vasapollo, A. Maffezzoli, L. Ambrosio, and L. Nicolais, *Journal of Applied Polymer Science*, 2008, **110**(4), 2453–2460.

[60] D. L. Teagarden and D. S. Baker, *European Journal of Pharmaceutical Sciences*, 2002, **15**(2), 115–133.

[61] F. Rol, C. Sillard, M. Bardet, J. R. Yarava, L. Emsley, C. Gablin, D. Léonard, N. Belgacem, and J. Bras, *Carbohydrate Polymers*, 2020, **229**, 115294.

[62] V. Kokol, M. Božič, R. Vogrinčič, and A. P. Mathew, *Carbohydrate Polymers*, 2015, **125**, 301–313.

[63] T. Hase, *Tables for organic spectrometry*, Otatieto, 1995.

[64] R. H. Newman, *Cellulose*, 2004, **11**, 45–52.

[65] A. L. M. Daneluti and J. d. R. Matos, *Brazilian Journal of Pharmaceutical Sciences*, 2013, **49**, 275–283.